Stochastic modelling of cavitation erosion in Francis runner

IOP Conf. Series: Earth and Environmental Science **240** (2019) 062017 doi:10.1088/1755-1315/240/6/062017

Stochastic modelling of cavitation erosion in Francis runner

Q Chatenet[1*], M Gagnon[2], L Tôn-Thât[2], M Fouladirad[3], E Remy[4], A S Tahan[1]

[1] Département de Génie Mécanique, École de Technologie Supérieure, 1100 Rue Notre-Dame Ouest, H3C 1K3, Montréal, QC, Canada
[2] Expertise – Performance, évolution et caractérisation des actifs, Recherche et innovation – Production, Institut de Recherche d'Hydro Québec, 1800 boul. Lionel-Boulet, J3X 1S1, Varennes, QC, Canada
[3] Modélisation et Sûreté des Systèmes, Université de Technologie de Troyes, 12 Rue Marie Curie, 10300 Troyes, France
[4] Département Performance, Risque Industriel, Surveillance pour la Maintenance et l'Exploitation, EDF R&D, 6 quai Watier, 78401 Chatou Cedex, France

***Email**: quentin.chatenet.1@etsmtl.net

Abstract. Reaction turbines, of which Francis turbines, constitute a large proportion of low and medium head turbines installed in hydropower plants. Managing these machines represents a real challenge in terms of efficiency, competitiveness and demands on the energy market. Turbines runner blades exhibit loss of performance from damage due to several reasons. One common source of damage is erosion due to the cavitation phenomenon. Indeed, at a given operating region, rapid changes of velocity can create bubbles in the water flow due to local low pressures. When cavitation bubbles reach pressure recovery, they collapse and may induce wear or erosion in these regions. Even if this phenomenon has been intensively studied in the past decades, cavitation erosion is not fully understood as it is driven by several parameters such as flow dynamic, turbine design, environment, or material properties. Some of these parameters can be studied in laboratory to compare materials resistance between each other. This article aims to model the cavitation by a stochastic model using erosion experimental data observed in the laboratory. The benefit of such models is to consider both the uncertainties and natural fluctuations of the phenomenon. With the proposed framework, the study will highlight the differences observed in cavitation erosion experiments of two common materials used to manufacture Francis's runners. This study is the first step in a project aiming at the prediction of turbines mass loss due to cavitation erosion on actual operating Francis turbines.

1. Introduction

Over the last few years, public and governmental policies have focused on increasing the production of energy from renewable sources to meet environmental objectives. These energy sources, such as solar or wind power, are known to be unpredictable and intermittent which may disturb the power network. Besides in the electricity market, sudden changes in the power demand can occur in the electricity market, forcing energy operators to adapt their production. Hence, to ensure the electrical grid stability, energy producers must rely on utilities capable of smoothing the power supply. Because of the relatively large range of operations of Francis units, they are particularly suitable to regulate power supply [1]. Meanwhile, depending on the operating region, cavitation, which represents an undesirable phenomenon, may appear at several locations of the Francis's runner [2]. This may occur when the local static pressure

of water reaches below its vapor pressure at local temperature. For high velocity regions of the runner, the local low pressure can result in the formation of small vapor bubbles which then collapse suddenly. If the created voids implode on a solid surface, such as a runner blade, the surface ends up with pitting corrosion [3]. This results in production of noise, vibration, the modification of the surface geometry of the blade and its surface condition. At the end it may lead to loss in the turbine overall efficiency. Over time, a Francis runner's exposed to erosive cavitation will lose material which requires costly periodic inspections and repairs. In order to optimize maintenance operations and to reduce periods of outage, there is a need to predict the erosive cavitation in hydro turbines.

A cavitation free operation is one of the most important issues for hydroelectric power plants [4]. Thus, turbine manufacturers must contractually prove the absence of cavitation for nominal operating points using CFD simulations. This work can be achieved by computing the dimensionless Thoma number (σ_i) which represents cavitation properties of the fluid

$$\sigma_i = \frac{p_{atm} - \rho g H_s - p_i}{\rho h H} \tag{1}$$

where p_{atm} is the atmospheric pressure, ρ the fluid density, g the gravitational acceleration, H_s the suction head of the turbine, H the net head and p_i the local static pressure [3]. Plant Thoma number (σ_p) represents the cavitation properties of the plant, which has a vapor pressure (p_v) corresponding fluid temperature

$$\sigma_p = \frac{p_{atm} - \rho g H_s - p_v}{\rho g H} \tag{2}$$

To ensure cavitation free operation, Thoma number must be lower than plant Thoma number at any location of the runner: $\sigma_p < \sigma_i$. Thus, optimization of hydraulic turbines design aiming to reduce cavitation is an active area of research [3,5,6]. While good progress has been made during the last decade, CFD simulations still face challenges when it comes to predicting cavitation erosion. Indeed, recent studies aiming to forecast cavitation erosion have shown satisfying qualitative results but stress that future work must be done to produce reliable quantitative ones [5]. Numerical models can predict the blade regions affected by erosive cavitation but are still not able to produce reliable results about the cavitation intensity and then the resulting material loss [6].

In this paper, we propose a different approach dealing with cavitation; instead of trying to reduce cavitation phenomena encountered in Francis's runners, we focus on modelling the resulting degradation. For this purpose, we use stochastic models and experimental data sets which allows to predict the future degradation state of the runner. Indeed, because of the replacement cost of such components and the necessity to operate them off design specifications, predicting their remaining useful lifetime represents a real asset for energy producers when it is time to schedule inspection and maintenance operations. As a proof of concept, the present study focuses on laboratory cavitation experimental data. This paper is structured as follows. First, the vibratory cavitation experiment is described to introduce the terminology used in the next sections. In section 2 we present the degradation model using non-homogeneous gamma process and its benefits compared to regression models. Next in section 4 we apply the degradation model on a real set of vibratory cavitation data. Finally, the conclusions of the results as well as furthers works are given in section 5.

2. Cavitation Test

The case study presented in the following sections relies on data from vibratory cavitation experiments performed in the laboratory. This experimental method, referred to as ASTM G32-06 standard, is mainly designed "*to compare the cavitation erosion resistance of different materials* [and / or] *to study in detail the nature and progress of damage in a given material*" [7]. Even if the experimental data cannot be directly transposed to hydraulic machines (due to the way the cavitation is generated in the test), the degradation mechanism is believed to be similar to the one observed in Francis's runners subject to cavitation erosion. In this study, cavitation erosion experiments have been performed in ultrasonic

equipment according to ASTM G32 standard. The specimens were held stationary below a vibrating horn at a distance of 0.5 ± 0.02 mm (indirect method). The frequency of vibration and the peak to peak displacement amplitude of the horn were 20 kHz and 50°µm. The experimental apparatus is shown in figure 1.

According to the process described in the ASTM standard, the test must follow the steps below:

- The specimen is immersed into a container filled with test liquid maintained at a specified temperature during the operation.
- The specimen is weighted accurately before testing begins and again during periodic interruptions of the test, in order to obtain a history of mass loss versus time.

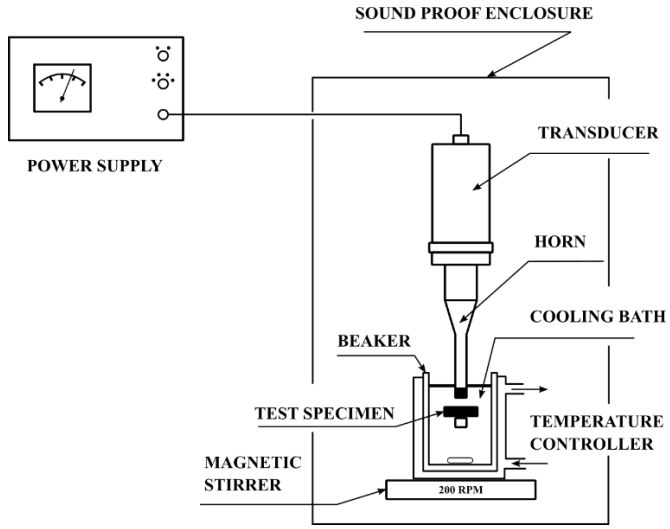

Figure 1. Schematic of vibratory erosion cavitation apparatus [7].

The following definitions, developed in the ASTM standard, will be used in the remaining part of this paper:

- **Nominal incubation time (A)**: the intercept of the time or exposure axis of the straight-line extension of the maximum-slope portion of the cumulative erosion-time curve; while this is not a true measure of the incubation stage, it serves to locate the maximum erosion rate line on the cumulative erosion versus time coordinates.
- **Maximum erosion rate (B)**: the maximum instantaneous erosion rate in a test that exhibits such a maximum followed by decreasing erosion rates.

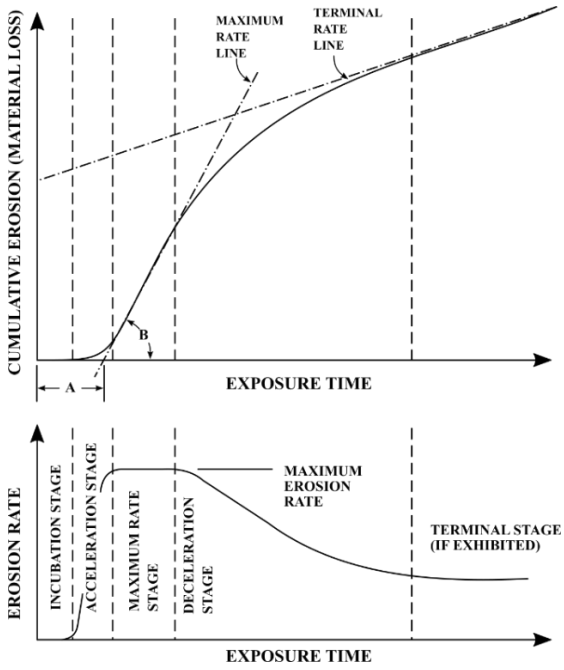

Note – A = nominal incubation time; tan(B) = maximum erosion rate

Figure 2. Characteristic stages of the erosion rate-time pattern, and parameters for representation of the cumulative erosion-time curve, adapted from [7].

3. Stochastic Model

3.1. Degradation Model

To describe degradation observations, two principal methods can be used by an analyst: regression models and stochastic processes. If we note $x_{i,j}$ the degradation level associated to test j at instant $t_{i,j}$, it is considered in regression models as an independent variable which is not influenced by previous degradation levels $x_{k,j}$, $k < i$. This means the way degradation data is collected and organized in paths is overlooked as well as the dynamic of degradation and its cumulative property over the time. In contrast, stochastic processes study the degradation path variability by considering the cumulative property of degradation. Thus, because of several sources of uncertainties and the natural variability of the cavitation phenomenon, the use of such probabilistic approach is legitimate. Moreover, a model update can be performed with stochastic processes using inspection results to provide more realistic predictions. Particularly, as pointed in the survey made by Noortwijk, Markov type of stochastic processes are well suited for modelling the temporal variability of degradation [8]. The most classical Markov processes used in reliability are the Wiener (also known Brownian motion) and gamma processes. A characteristic feature of the first one – in the context of degradation – is that the degradation alternately increases and decreases over time (non-monotone locally), even with an increasing trend (Brownian motion with drift). On the contrary, gamma process has only non-negative increments over time which means the degradation is strictly monotone. Indeed, gamma process paths can be thought as the accumulation over time of an infinite number of tiny increments. This feature makes the gamma process suitable to model gradual damage accumulating over time as observed in our cavitation data (see figure 3) [8].

First, let us introduce the mathematical basis of the gamma process, based on the gamma distribution. A random quantity X has a gamma distribution, denoted $Ga(v,u)$, with $v,u > 0$ the shape parameter and the rate parameter respectively, if its probability density function is given by:

$$f_X(x) = Ga(x|v,u) = \frac{u^v}{\Gamma(v)} x^{v-1}\, \mathrm{e}^{-ux} I_{\mathbb{R}_+^*}(x), \tag{3}$$

where $I_A(x) = 1$ for $x \in A$ and $I_A(x) = 0$ for $x \notin A$, and $\Gamma(a) = \int_{z=0}^{+\infty} z^{a-1}e^{-z}dz$ is the gamma function for $a > 0$. Note that another standard parameterization of the gamma distribution in the literature is (α, β) with $\alpha = v$ and $\beta = \frac{1}{u}$. In that case, β is called scale parameter and α is called shape parameter. The gamma process $\{X(t),\ t \geq 0\}$ with shape function $v(t) > 0$ and rate parameter $u > 0$ has the following properties:

- $X(0) = 0$,
- $X(\tau) - X(t) \sim Ga(v(\tau) - v(t), u)$ for all $\tau > t > 0$,
- $X(t)$ has independent increments. The future degradation is independent of the past degradation.

The two principal choices for shape function $v(t)$ are: the power shape function, $v(t) = vt^b$ with $v, b > 0$ and the exponential shape function $v(t) = e^{-vt} - 1$, with $v > 0$ [9]. Empirical studies and engineering knowledge show the expected degradation over time is often proportional to a power law [8]. From an engineering point of view, it expresses how the mean degradation increases over time. When $b = 1$, the gamma process is said homogeneous; for $b \neq 1$, the gamma process is non-homogeneous. Considering the degradation evolution during our cavitation test, we decided to use the gamma shape function expressed with a power law.

The expectation and the variance of gamma process are given respectively in equation (4).

$$\mathbb{E}\big(X(t)\big) = \frac{v(t)}{u} = \frac{vt^b}{u}, \qquad \mathbb{V}\big(X(t)\big) = \frac{v(t)}{u^2} = \frac{vt^b}{u^2} \tag{4}$$

In our case, $X(t)$ denotes the cumulative mass loss of material over time t during a vibratory cavitation test.

3.2. Parameter Estimation for the Gamma Process

We introduce here some notations. We observe m independent and identically distributed copies of the stochastic process as described above. In the case study, m expresses the number of tests performed and n_j the number of successive measurements taken during test j, $1 \leq j \leq m$. Then, the j^{th} path is observed n_j times at the instants $t_0 < t_{1,j} < \cdots < t_{n_j,j}$. We adopt the following notations in the remaining of the paper, for all $1 \leq j \leq m$:

- $t_{0,j} = t_0 = 0$;
- $x_{0,j} = 0$, at t_0 there is no degradation;
- $\delta_{i,j} = x_{i,j} - x_{i-1,j}$, the increment of degradation between inspections times $t_{i-1,j}$ and $t_{i,j}$;
- $\boldsymbol{D}_{obs} = \cup_{j=1}^{m} \cup_{i=1}^{n_j} \{(t_{i,j}, x_{i,j})\}$, the set of all observed degradation data.

Degradation model parameters can then be estimated using the maximum likelihood estimator (MLE). The gamma process likelihood function $\mathcal{L}$ is given in equation (5). This method consists in choosing the model parameters' values which maximize the likelihood function $\mathcal{L}$ given observed data. Intuitively, this selects the parameter values that make the data most probable. For convenience, we prefer to maximize the log-likelihood function ℓ in equation (6) using optimization methods.

$$\mathcal{L}(u, v, b|\boldsymbol{D}_{obs}) = \prod_{j=1}^{m} \prod_{i=1}^{n_j} \frac{u^{v\left[t_{i,j}^b - t_{i-1,j}^b\right]}}{\Gamma\left(v\left[t_{i,j}^b - t_{i-1,j}^b\right]\right)} \delta_{i,j}^{v\left[t_{i,j}^b - t_{i-1,j}^b\right]-1} \mathrm{e}^{-u\delta_{i,j}} \tag{5}$$

$$\begin{aligned}\ell(u,v,b|\boldsymbol{D}_{obs}) &= \log\big(\mathcal{L}(u,v,b|\boldsymbol{D}_{obs})\big)\\ &= \sum_{j=1}^{m}\sum_{i=1}^{n_j} v\big[t_{i,j}^{b}-t_{i-1,j}^{b}\big]\log(u) - \log\big[\Gamma\big(v\big[t_{i,j}^{b}-t_{i-1,j}^{b}\big]\big)\big]\\ &+ \big(v\big[t_{i,j}^{b}-t_{i-1,j}^{b}\big]-1\big)\log\big(\delta_{i,j}\big) - u\delta_{i,j}\end{aligned} \tag{6}$$

By differentiating the log-likelihood function ℓ with respect to the three variables, the MLE $(\hat{u},\hat{v},\hat{b})$ of (u,v,b) consists in the solution of the follow set of equations:

$$\hat{u} = \hat{v}\,\frac{\sum_{j=1}^{m}\sum_{i=1}^{n_j}[t_{i,j}^{\hat{b}}-t_{i-1,j}^{\hat{b}}]}{\sum_{j=1}^{m}\sum_{i=1}^{n_j}\delta_{i,j}} = \hat{v}\frac{\sum_{j=1}^{m}t_{n_j,j}^{\hat{b}}}{\sum_{j=1}^{m}x_{n_j,j}} \tag{7}$$

$$\sum_{j=1}^{m}\sum_{i=1}^{n_j}[t_{i,j}^{\hat{b}}-t_{i-1,j}^{\hat{b}}]\Big\{\psi\Big(\hat{v}\Big[t_{i,j}^{\hat{b}}-t_{i-1,j}^{\hat{b}}\Big]\Big)-\log(\delta_{i,j})\Big\} = \sum_{j=1}^{m}(t_{n_j,j}^{\hat{b}})\log\left(\hat{v}\frac{\sum_{j=1}^{m}t_{n_j,j}^{\hat{b}}}{\sum_{j=1}^{m}x_{n_j,j}}\right), \tag{8}$$

$$\begin{aligned}&\sum_{j=1}^{m}\sum_{i=1}^{n_j}\hat{v}\Big[t_{i,j}^{\hat{b}}\log\big(t_{i,j}\big)-t_{i-1,j}^{\hat{b}}\log\big(t_{i-1,j}\big)\Big]\Big[\psi\Big(\hat{v}\Big[t_{i,j}^{\hat{b}}-t_{i-1,j}^{\hat{b}}\Big]\Big)-\log\big(\delta_{i,j}\big)\Big]\\ &= \sum_{j=1}^{m}\Big(\hat{v}t_{n_j,j}^{\hat{b}}\log\Big(t_{n_j,j}\Big)\Big)\log\left(\hat{v}\frac{\sum_{j=1}^{m}t_{n_j,j}^{\hat{b}}}{\sum_{j=1}^{m}x_{n_j,j}}\right)\end{aligned} \tag{9}$$

where the function $\psi(x)$ is the derivative of the logarithm of the gamma function, also called di-gamma function:

$$\psi(x) = \frac{\Gamma'(x)}{\Gamma(x)} = \frac{\partial\log\Gamma(x)}{\partial x} \tag{10}$$

Hence, estimators $\hat{v}$ and $\hat{b}$ can be either numerically computed by solving the last two equations or by computing the MLE with respect to $\hat{v}$ and $\hat{b}$. Then, $\hat{u}$ can be computed using equation (7). Both methods are numerical and imply an optimization using proper computing tools.

3.3. Simulation

One benefit of modelling a component degradation is the ability to predict its future deterioration state. Hence, for a given degradation threshold ρ, the remaining useful lifetime RUL of a component needs to be computed. If $X(t)$ represents the degradation accumulated by a component on the interval $[0,t]$, we consider the component in failed state as soon as the degradation is beyond threshold ρ. We call the time-to-failure of the component, the hitting time τ_ρ expressed in equation (11).

$$\tau_\rho = inf\{t \geq 0 : X(t) \geq \rho\} \tag{11}$$

For estimated degradation paths, $\tau_{\rho,j}$ corresponds to the time $t_{i,j}$ the degradation level $X(t_{i,j})$ crosses threshold ρ. Computing all $\tau_{\rho,j}$, $1 \leq j \leq m$, allows then to determine asymptotically the hitting time distribution of the component degradation level of a large number of simulated paths. We refer the reader to [8,9] for further details on this topic.

If we want to generate values of the process on the discrete time range $[0,T]$, at the instants $t_i = i \times \Delta T$, $i = 1, \ldots, 2^k$, where $\Delta = 2^{-k}, k \in \mathbb{N}_+^*$, an efficient method to simulate gamma process sample paths

(with respect to the estimated parameters $(\hat{u}, \hat{v}, \hat{b})$) is the gamma sequential sampling (GSS) presented in the following algorithm [10].

$G(0) = 0$;
$h = 2^{-k}T$;
For $i = 0$ to 2^k,
Generate $Q \sim Ga\left(\hat{v}[(i+1)h]^{\hat{b}} - \hat{v}[ih]^{\hat{b}}, \hat{u}\right)$;
$G(ih) = G\left((i-1)h\right) + Q$;
Next i

4. Case Study

4.1. Materials Tested

In the present study, the materials used are ASTM A27 and E309L. These two materials have been chosen because of their common use in the fabrication process of Francis's runners. ASTM A27 has been extensively used to build runners since the 1950's. The samples used (1-inch diameter cylinder) have been extracted from a blade casting. Then, E309L is nowadays most commonly used for welding material to repair fatigue cracks or cavitation damages in hydraulic turbines. The samples have been extracted from a bulk sample made of several welding beads. The vibratory cavitation test has been performed on these two materials according to the process described in section 2. To capture the variability of the experimental process and material properties, two replications have been done for E309L and at least one for ASTM A27. It results is a total of 49 measurements for E309L and 25 for ASTM A27. Because of limited available data, the analyst must be aware of the larger parameter estimation uncertainties associated with smaller datasets.

From an industrial point of view, we decided to focus on the acceleration stage (as denoted in the ASTM vibratory cavitation test presented above), as the incubation stage is not currently observed in the vibratory and acoustic apparatus used for cavitation monitoring systems. Indeed, even if, on the one hand, CFD simulations face difficulties to estimate the cavitation intensity on real operating turbines, on the other hand, experimental knowledge implies that cavitation intensity occurring in real turbines is probably much higher than the one generated in the laboratory with vibrating test equipment. The differences of cavitation intensities observed can partially explain why the incubation stage is not seen in the degradation dynamic of real prototypes. From this perspective, only the acceleration stage was modeled. Then, incubation time $t_{inc,j}$ for each test j has been graphically determined with the slope of the degradation curve (as detailed in the ASTM vibratory cavitation standard). The results are shown in table 1. Degradation path results are shown in figure 3. Incubation and acceleration stages are represented with the darker and lighter areas respectively.

Table 1. Incubation time $t_{inc,j}$ for vibratory cavitation tests performed on usual materials.

Test number	Material	
	ASTM A27	E309L
1	75 min	150 min
2	105 min	180 min
3	-	180 min

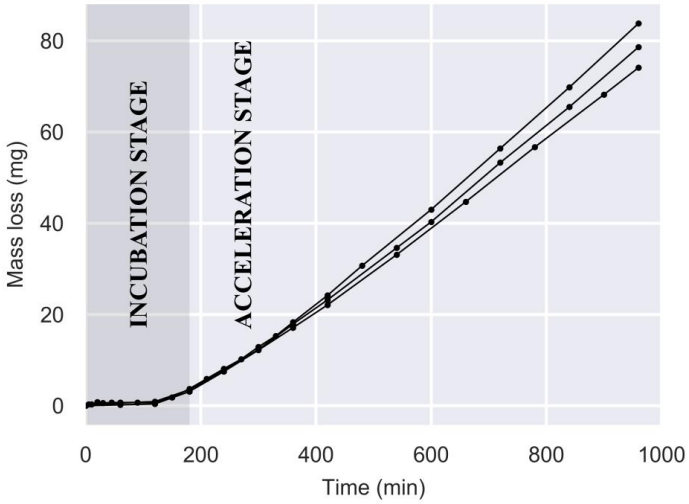

Figure 3. Degradation path results for E309L material.

For simplicity matters and to make data consistent with MLE equations, acceleration stage datasets have been shifted to have $t_{0,j} = t_{inc,j}$ and $x_{0,j}(t_{0,j})$. This transformation has been done shifting the coordinates origin to $t_{new,j} = t_{inc,j}$ along the time axis and $x_{new,j} = x(t_{new,j})$ along the degradation axis.

4.2. Statistical Analysis

As pointed out in the previous section, regression models allow to perform quick statistical analysis which is useful to determine initial guess in the optimization scheme used to perform MLE. Four classic regression models have been tried on our degradation data: logarithmic, linear, polynomial (order 2 and 3) and power law using R software. The power law model $X(t) = at^c$ shows the best fit according to AIC (Akaike Information Criterion estimates relative quality of statistical models for a given dataset [11]) values with a power $c = 1.15 > 1$ statistically significantly and has been used to perform MLE optimization.

4.3. Parameter Estimation

Equation (7) has been used to express $\hat{u}$ with respect to estimated parameters $\hat{v}$ and $\hat{b}$. Indeed, instead of performing the MLE on the three gamma process parameters, the log-likelihood function ℓ has been maximized only with respect to parameters $\hat{v}$ and $\hat{b}$ which reduces optimization difficulties (one dimension has been removed in the log-likelihood function ℓ). Initial guess on $\hat{b}$ parameter is taken from previous statistical analysis results. The `Optimization and Root Finding` library of `Scipy` [12] has been used to perform the MLE. To avoid numerical issues due to the gamma function evaluation encountered in equation (9), time datasets have been multiplied by a k factor to numerically decrease the value of time increments since $\Gamma(n+1) = n!$ for $n \in \mathbb{N}$ may result in overly large values of $\Gamma(x)$. For this study, we took $k = 1/200$. For consistent results and comparison matter, time transformation must be done for all datasets and k-factor must remain constant in the whole study.

Two shape functions have been studied in this section. First, we took the simpler case with $v(t) = vt$, the linear shape function (or $b = 1$ in $v(t) = vt^b$). It supposes the degradation speed is constant over time. Then we used non-homogeneous shape function $v(t) = vt^b, b \neq 1$. MLE has been computed for the two shape functions $v(t)$ to estimate gamma process parameters in the two cases.

4.4. Simulation – Model Comparison

A convergence study on the mean and variance of simulated paths has been performed to determine the necessary number of paths m to reach an asymptotic behaviour. This study showed that the asymptotic behaviour is reached for more than 8,000 paths. In figure 4, 10,000 paths have been simulated over discrete time [0, 1500] min. An arbitrary degradation threshold (dashed black line in figure 4) has been set to $100\,mg$ to illustrate the RUL computation using simulated paths. Probability densities of degradation levels at times 360, 600 and 960 min have been computed using simulated paths and are shown in figure 5. The black dots in figure 5 represent the experimental degradation levels at 360, 600 and 960 min respectively for the three performed tests. Figure 6 shows probability densities of hitting time to the threshold $\rho = 100\,mg$.

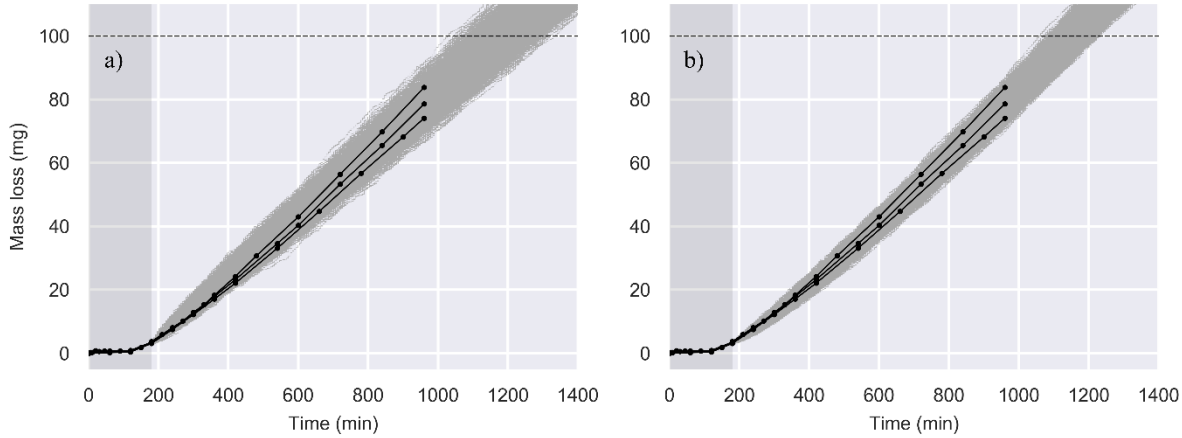

Figure 4. a) Homogeneous and **b)** Non-homogeneous gamma process simulation at acceleration stage – 10,000 simulated paths. Black lines represent experimental degradation paths.

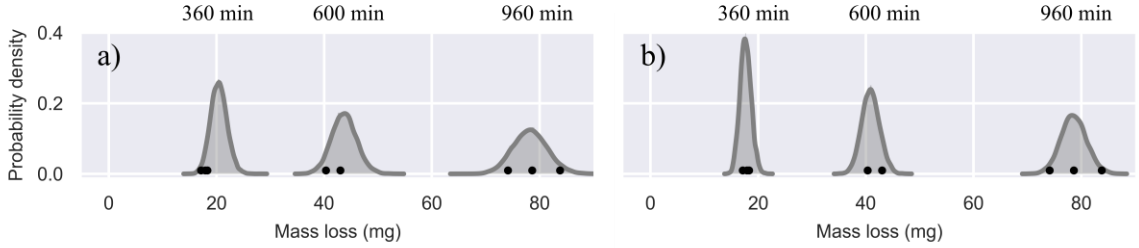

Figure 5. Probability densities of degradation level at 360, 600 and 960 min for **a)** Homogeneous and **b)** Non-homogeneous gamma process simulation.

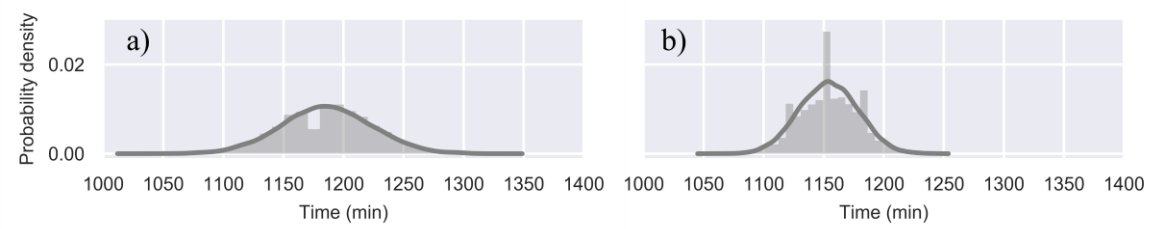

Figure 6. Probability densities of hitting times for $\rho = 100\,mg$ **a)** Homogeneous and **b)** Non-homogeneous gamma process simulation. The kernel density estimation is given by the grey curve.

The results in figure 4 and 5 show a better modeling using non-homogeneous shape parameter. MLE gives in this case a power $\hat{b} = 1.13$ which is consistent with the regression results using power law model (estimates of rate and shape parameters are respectively $\hat{u} = 13.1, \hat{v} = 209$ for non-homogeneous gamma process). In figure 5, we can observe that the probability densities of non-

homogeneous gamma process simulation paths are more centered on experimental degradation levels and the range is tighter than the ones found for homogeneous gamma process. It reflects the degradation dynamic is better modelled with non-homogeneous gamma process.

5. Conclusion

This paper shows a stochastic model for vibratory cavitation test modelled with homogeneous and non-homogeneous gamma process. This model is suitable for a cumulative and monotone degradation such as erosive cavitation. Paths simulations have been computed to compare and graphically validate gamma process parameter estimations. This work is the first step of prediction of erosive cavitation encountered in Francis's runner using stochastic models. Future work must be done to quantify parameters estimation uncertainties. For this purpose, (non-)parametric bootstrap technique will be studied [13]. Because of the small data set and the availability of other sources of information about cavitation erosion, a Bayesian framework should be well suited to combine multiple sources of information [14]. Such framework would make it possible to also include information like expert knowledge, monitoring data and results from the numerical simulation.

Acknowledgments

This study was carried out with the financial support of the Canadian research internship program, MITACS-Accelerate.

References

[1] Alligne S, Nicolet C, Tsujimoto Y and Avellan F 2014 Cavitation surge modelling in Francis turbine draft tube *J Hydraul Res* **52** pp 399–411.
[2] Escaler X, Egusquiza E, Farhat M, Avellan F and Coussirat M 2006 Detection of cavitation in hydraulic turbines. *Mech Syst Signal Process* **20** pp 983–1007.
[3] Celebioglu K, Altintas B, Aradag S and Tascioglu Y 2017 Numerical research of cavitation on Francis turbine runners *Int J Hydrog Energy* **42** 17771–81.
[4] Brennen CE 2014 *Cavitation and bubble dynamics* Cambridge University Press
[5] Krumenacker L, Fortes-Patella R and Archer A 2014 Numerical estimation of cavitation intensity *IOP Conf. Ser. Earth Environ. Sci.* **22** p 052014.
[6] Gohil PP and Saini RP 2016 Numerical study of cavitation in Francis turbine of a small hydro power plant *J Appl Fluid Mech* **9**.
[7] ASTM G. 32-09 2003 Standard test method for cavitation erosion using vibratory apparatus *Annu Book ASTM Stand ASTM*
[8] Van Noortwijk JM 2009 A survey of the application of gamma processes in maintenance *Reliab Eng Syst Saf* **94** pp 2–21.
[9] Kahle W, Mercier S and Paroissin C 2016 *Degradation processes in reliability* John Wiley & Sons
[10] Avramidis A N, L'Ecuyer P and Tremblay A 2003 Efficient simulation of gamma and variance-gamma processes *Proc. Winter Simul. Conf.* **1** pp 319-326
[11] Akaike H 1987 *Factor analysis and AIC Sel. Pap. Hirotugu Akaike* Springer pp 371-386
[12] Optimization and root finding (scipy.optimize) — SciPy v1.0.0 Reference Guide n.d. https://docs.scipy.org/doc/scipy/reference/optimize.html (accessed March 27, 2018).
[13] Freedman DA 1981 Bootstrapping regression models *Ann Stat* **9** pp1218–1228.
[14] Bernardo JM and Smith AF 2001 *Bayesian theory* Wiley Series in probability and statistics